An Explicit Quantum Chemical Method for Modeling Large Solvation Shells Applied to Aminocoumarin C151

Johannes Neugebauer,*,† Christoph R. Jacob,†,§ Tomasz A. Wesolowski,‡,|| and Evert Jan Baerends*,†

Theoretical Chemistry, Vrije Universiteit Amsterdam, De Boelelaan 1083, 1081 HV Amsterdam, The Netherlands, and Department of Physical Chemistry, University of Geneva, 30 quai Ernest-Ansermet, CH-1211 Geneva 4, Switzerland

Received: May 31, 2005; In Final Form: July 5, 2005

The absorption spectra of aminocoumarin C151 in water and *n*-hexane solution are investigated by an explicit quantum chemical solvent model. We improved the efficiency of the frozen-density embedding scheme, as used in a former study on solvatochromism (*J. Chem. Phys*. **2005**, *122*, 094115) to describe very large solvent shells. The computer time used in this new implementation scales approximately linearly (with a low prefactor) with the number of solvent molecules. We test the ability of the frozen-density embedding to describe specific solvent effects due to hydrogen bonding for a small example system, as well as the convergence of the excitation energy with the number of solvent molecules considered in the solvation shell. Calculations with up to 500 water molecules (1500 atoms) in the solvent system are carried out. The absorption spectra are studied for C151 in aqueous or *n*-hexane solution for direct comparison with experimental data. To obtain snapshots of the dye molecule in solution, for which subsequent excitation energies are calculated, we use a classical molecular dynamics (MD) simulation with a force field adapted to *first-principles* calculations. In the calculation of solvatochromic shifts between solvents of different polarity, the vertical excitation energy obtained at the equilibrium structure of the isolated chromophore is sometimes taken as a guess for the excitation energy in a nonpolar solvent. Our results show that this is, in general, not an appropriate assumption. This is mainly due to the fact that the solute dynamics is neglected. The experimental shift between *n*-hexane and water as solvents is qualitatively reproduced, even by the simplest embedding approximation, and the results can be improved by a partial polarization of the frozen density. It is shown that the shift is mainly due to the electronic effect of the water molecules, and the structural effects are similar in *n*-hexane and water. By including water molecules, which might be directly involved in the excitation, in the embedded region, an agreement with experimental values within 0.05 eV is achieved.

1. Introduction

The theoretical description of solvent effects on molecular properties, e.g., absorption spectra, requires the consideration of both specific and nonspecific solvent effects. For this purpose, many studies employing continuum solvation models to cover the dielectric effect of a solvent are augmented with additional explicit solvent molecules to describe, e.g., the effect of hydrogen bonding on excitation energies of solvatochromic dyes.[1,2] However, such hybrid models are often based on optimized (static) structures of the dye−water clusters, and they are applied to model the effect of a dynamical solvent. This problem is avoided in explicit models such as Car−Parrinello molecular dynamics (CPMD) schemes[3] in combination with time-dependent density functional theory (TDDFT) calculations, as has been demonstrated for *s*-tetrazine[4] and acetone.[5,6] To overcome the high demands in computer time for larger systems, the CPMD approach can be combined with a classical molecular-mechanics treatment of the solvent.[7,8]

Recently, we could show that the frozen-density embedding scheme[9] provides a valuable tool for the calculation of solvatochromic shifts.[10] In this scheme, the Kohn−Sham-like, one-electron equations for embedded orbitals, eqs 20 and 21 in ref 9, integrated within the general framework of linear response TDDFT[11,12] are used to evaluate the electronic excitation energies localized on a predefined subsystem. Together with an appropriate method to generate snapshots of the molecule in solution, e.g., CPMD, the scheme combines the advantages of an explicit and entirely quantum chemical description of the whole system (comprising the chromophore and solvent molecules), as in CPMD-TDDFT calculations, and of a restricted orbital space, as in QM/MM methods. The last point is of particular importance for the computational efficiency and the interpretation of the solute properties.[10,13]

In this study, we present an improved implementation of the embedding scheme, in which the computational cost is considerably reduced by using (i) a simplified sum-of-fragment density for the frozen system and (ii) an efficient integration scheme for the outer part of the environment. This leads to an approximately linear scaling of the CPU time with the number of solvent molecules. Calculations with more than 1000 atoms in the frozen system are easily possible because the prefactor for the linear increase in CPU time is very low. Similar to the

* Corresponding authors. E-mail: jneugeb@chem.vu.nl (J.N.); baerends@chem.vu.nl (E.J.B.).
† Vrije Universiteit Amsterdam.
§ E-mail: jacob@chem.vu.nl.
‡ University of Geneva.
|| E-mail: Tomasz.Wesolowski@chiphy.unige.ch.

10.1021/jp0528764 CCC: $30.25
Published on Web 08/09/2005

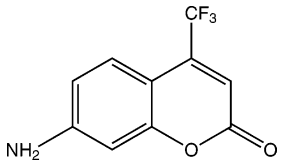

Figure 1. Structure of aminocoumarin C151.

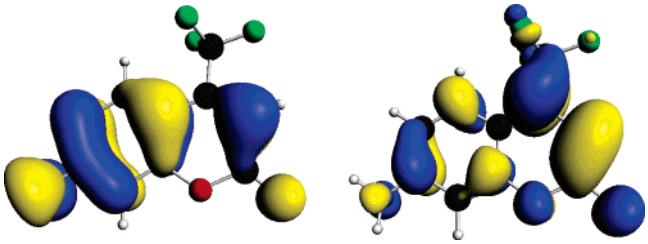

Figure 2. Isosurface plots of HOMO (π) and LUMO (π^*) orbitals of aminocoumarin C151.

studies in refs 14 and 15, we apply a sequential scheme of a classical molecular dynamics (MD) simulation, followed by a *first-principles* calculation of the excitation energies for snapshots extracted from this simulation.

With this approach, we study the absorption spectrum of aminocoumarin C151, which is shown in Figure 1. There has been considerable interest in coumarin dyes because of their importance as laser dyes in the near-ultraviolet to green part of the spectrum[16] and as environmental or solvent probes, which are based on the strong dependence of their absorption and fluorescence characteristics on the surrounding media (see, e.g., ref 17).

The lowest singlet excitation in these aminocoumarins is a $\pi \rightarrow \pi^*$ excitation, which shows a pronounced red shift in polar solvents.[18−20] Isosurface plots of the orbitals involved in this transition, in the case of aminocoumarin C151, are shown in Figure 2. Former theoretical studies on the absorption properties and excited states of these molecules in solution mainly used continuum solvation models.[21−24] Especially in ref 21, the importance of specific and inhomogeneous interactions between solvent and solute, which are necessarily neglected in continuum models, has been underlined. In ref 8, the excitation energies have been calculated for C151 in water and acetonitrile using QM/MM-CPMD. Solvent shifts have then been computed with respect to the vertical excitation energy of the molecule in vacuo (as a model for a nonpolar solvent), and they were found to reproduce the experimental shifts between nonpolar and polar solvents quite well. A direct comparison of the simulations in acetonitrile and water, however, indicates a shift of 0.11 eV between these two solvents, compared with an experimental shift of <0.01 eV.[18] Moreover, it is known from CPMD simulations[10] or studies of the vibrational broadening of absorption bands[25−27] that vertical excitation energies and band maxima for gas-phase molecules often differ by 0.1−0.2 eV; so, this aspect should be taken into account in the calculation of shifts in excitation energies. Hence, in the present study, we want to assess the quality of the frozen-density embedding scheme in combination with a classical MD simulation for the calculation of solvatochromic shifts. For a direct comparison of a polar and a nonpolar solvent, we compare simulations in *n*-hexane and in water.

After a brief outline of the frozen-density embedding formalism and of the computational details in section 2, a discussion of the improved numerical integration scheme for the frozen region is presented in section 3. In section 4, we investigate the ability of the embedding scheme to reproduce specific interactions due to hydrogen bonding for aminocoumarin C151. A study on the convergence of the excitation energies with respect to the number of solvent molecules in the outer solvation shells, which still might contribute to the nonspecific solvent effects, is presented in section 5. A comparison and validation of different types of embedding approaches as well as a closer look at the origin of the shift in our simulation are presented in section 6. In that section, we also present a combination of the sum-of-fragment approach for the frozen-density and freeze-and-thaw technique.[28] The results of the final spectrum simulation are shown in section 7. Concluding remarks follow in section 8.

2. Methodology

In the orbital-free embedding formalism,[9] the electron density of the embedded subsystem (ρ_I) in a given microscopic environment, which is represented by means of the frozen electron density (ρ_{II}) and a set of nuclear charges ($Z_{A_{II}}$) at the corresponding positions ($\mathbf{R}_{A_{II}}$), is derived from Kohn−Sham-like one-electron equations. The effective potential in these equations is derived from the requirement that the total density, $\rho_{total} = \rho_I + \rho_{II}$, of the system is obtained, which minimizes the total energy, from an optimization process in which the environment density ρ_{II} is kept frozen. On the assumption that the complementary ρ_I is positive definite and is noninteracting v_s-representable (i.e., is associated with a ground-state wave function of the Kohn−Sham Hamiltonian[29]), one can derive Kohn−Sham-type equations, i.e., one-electron equations with a multiplicative effective potential depending explicitly on ρ_I and ρ_{II}. In these equations, eqs 20 and 21 in ref 9, the effect of ρ_{II} is folded into the effective potential for the ρ_I system. We refer to this effective potential and the corresponding equations as KSCED (Kohn−Sham approach with constrained electron density). The KSCED effective potential contains the same terms as those the isolated system I would contain (nuclear attraction and electron Coulomb and exchange-correlation potentials), plus an additional (embedding) component which reads

$$V_{emb}^{eff}[\mathbf{r},\rho_I,\rho_{II}] = \sum_{A_{II}} -\frac{Z_{A_{II}}}{|\mathbf{r}-\mathbf{R}_{A_{II}}|} + \int \frac{\rho_{II}(\mathbf{r}')}{|\mathbf{r}'-\mathbf{r}|}\,d\mathbf{r}' + \frac{\delta E_{xc}[\rho]}{\delta\rho}\bigg|_{\rho=\rho_I+\rho_{II}} - \frac{\delta E_{xc}[\rho]}{\delta\rho}\bigg|_{\rho=\rho_I} + \frac{\delta T_s[\rho]}{\delta\rho}\bigg|_{\rho=\rho_I+\rho_{II}} - \frac{\delta T_s[\rho]}{\delta\rho}\bigg|_{\rho=\rho_I} \quad (1)$$

where the exchange-correlation ($E_{xc}[\rho]$) and kinetic-energy ($T_s[\rho]$) functionals are defined in the Kohn−Sham formulation of density functional theory (DFT). We may also write the kinetic-energy part of the potential as the functional derivative $\delta T_s^{nadd}[\rho_I,\rho_{II}]/\delta\rho_I$ of the nonadditive kinetic-energy functional

$$T_s^{nadd}[\rho_I,\rho_{II}] = T_s[\rho_I+\rho_{II}] - T_s[\rho_I] - T_s[\rho_{II}] \quad (2)$$

Note that the effective embedding potential given in eq 1 is not linear in either ρ_I or ρ_{II}. In practical calculations, it must therefore be recalculated in each self-consistent field (SCF) step. The system-independent form of the effective potential in one-electron equations for embedded orbitals was introduced originally by Cortona.[30] In his subsystem formulation of density functional theory, all components of the total electron density (ρ_I and ρ_{II} in our case) are subject to variational calculations; i.e., none of them are subject to additional simplifications or

approximations as applied in this work. We use the gradient-dependent approximation for $T_s^{nadd}[\rho_I,\rho_{II}]$ based on dedicated numerical tests in the case of weakly overlapping ρ_I and ρ_{II}.[28] Studies[31,32] of the accuracy of various approximations to $T_s^{nadd}[\rho_I,\rho_{II}]$ in the case of weakly overlapping pairs of electron densities, ρ_I and ρ_{II}, showed that the most accurate nonadditive kinetic-energy functional (and the associated functional derivative) has the same analytic form of the enhancement factor $F(s)$ as that of the exchange functional of Perdew and Wang[33], but it is reparametrized for the kinetic energy by Lembarki and Chermette.[34] Its complete form reads

$$F_{LC94}(s) = \frac{1 + 0.093907s\,\mathrm{arcsinh}(76.32s) + (0.26608 - 0.0809615e^{-100s^2})s^2}{1 + 0.093907s\,\mathrm{arcsinh}(76.32s) + 0.57767 \times 10^{-4}s^4} \quad (3)$$

The exchange-correlation component of the effective embedding potential is approximated using the Becke−Perdew−Wang (BPW91) exchange-correlation functional.[33,35] A time-dependent linear response generalization of the frozen-density embedding scheme has been devised in ref 11 and is implemented in the Amsterdam Density Functional (ADF) package.[36,37] It allows the calculation of excitation energies, assuming that the excitations are localized on subsystem I.

Absorption spectra are simulated by calculating excitation energies for a number of solvent configurations obtained as snapshots from a classical MD simulation. For these MD simulations, the general Amber force field (GAFF)[38] and the TIP3P water model[39] were employed using the TINKER package[40,41] to run the calculations. Partial atomic charges for the aminocoumarin dye were taken from a multipole-derived charge analysis (reconstructing monopole, dipole, and quadrupole moments)[42] based on a SAOP (statistical averaging of molecular orbital potentials) calculation, as described below. For *n*-hexane as a solvent, we used a mean value of these multipole-derived charges for an optimized structure. To improve the force field parameters for bond stretching and valence angle bending, the equilibrium bond lengths and bond angles from an optimized structure of C151 were used. The Becke−Perdew functional, dubbed BP86,[35,43] was employed in combination with the TZP basis set from the ADF basis set library[36] for this structure optimization and the calculation on *n*-hexane. This ensures that the BP86/TZP equilibrium bond distances and angles of aminocoumarin C151 are indeed the minima of the corresponding potential functions in the classical force field simulation. The radial distribution functions (RDF) for $N-O_{water}$ and $O_{carbonyl}-O_{water}$ for the classical simulation in water have been compared to the corresponding results in ref 8 based on a QM/MM-CPMD approach, and the characteristic features were reproduced.

All density functional calculations have been performed using the Amsterdam Density Functional (ADF) package.[36,37] The SAOP potential[44−46] is used with the TZP basis set to calculate vertical TDDFT excitation energies because it is well-suited for describing both valence and Rydberg excited states; this is in contrast to normal generalized gradient approximation (GGA) potentials, which introduce additional problems by artificially placing Rydberg excitations at energies that are much too low.[47] The electron density of the solvent, which enters eq 3 as ρ_{II}, was calculated as a sum of molecular densities of solvent molecules obtained with LDA/DZP.[10] To check the effect of the basis set for the solvent system, the DZ and TZP basis sets were also used for the frozen system.

3. Improved Efficiency for Frozen-Density Embedding Calculations

A great advantage of the orbital-free embedding calculations in comparison to supermolecule calculations is the restriction to the orbital space of the embedded system. As a consequence, the dimensions of the Fock matrix and of the TDDFT eigenvalue problem (see, e.g., refs 48−50) are independent of the system size.

The bottleneck in frozen-density calculations for large solvation shells is the generation of the solvent density, which in principle requires a converged SCF for the system to be frozen in the embedding calculation. In ref 10, it was shown that this can be avoided without significant loss of accuracy in the excitation energies by using a superposition of molecular densities for the solvent. This approach made it possible to apply the embedding scheme to excitations of systems solvated by several hundreds of solvent molecules. For ground-state properties, similar construction methods of approximate environmental densities have been employed.[51−54]

However, the first implementation, used in ref 10, still showed a rather strong increase of the CPU time with increasing system size. Calculations with up to 300 water molecules could be carried out, but statistical analyses with solvent shells of this size were out of reach.

We have now implemented a version of the frozen-density embedding which is improved in three respects: (i) the generation of the sum-of-fragment density has been made more efficient, (ii) the cost of the numerical integration has been significantly decreased by using a reduced integration grid, and (iii) linear scaling techniques are employed.

ADF uses a numerical integration scheme for evaluating the matrix elements of the Coulomb and exchange-correlation potentials.[37] As many steps scale linearly with the number of grid points, the generation of an efficient integration grid is of great importance to speed up the calculations.

Besides the integrals that are needed in the calculations of the isolated system I, the matrix elements of the embedding potential are also necessary in KSCED calculations. These matrix elements are given by

$$\langle\chi_i|V_{emb}^{eff}|\chi_j\rangle = \int \chi_i^*(\mathbf{r})\, V_{emb}^{eff}(\mathbf{r})\, \chi_j(\mathbf{r})\, d\mathbf{r} \quad (4)$$

where V_{emb}^{eff} is the embedding potential given in eq 1 and $\chi_{i,j}$ are the Slater-type orbital (STO) basis functions that are used in the calculation of the nonfrozen system and are usually centered only on the atoms in the nonfrozen system. The integration grid should be constructed in such a way that only the region in space where the integrand is not negligible is covered.

Among the different components of the embedding potential, the integration of the Coulomb potential for the frozen system puts the most severe requirements on the integration grid because the singularities of the Coulomb potential at the nuclei of the frozen system need to be integrated accurately. We therefore concentrate in the following on this contribution to the embedding potential. The previous implementation of the KSCED scheme in ADF used the same integration grid that would be employed in a full supermolecular calculation to avoid problems in this step. However, this integration grid is much larger than necessary, especially in calculations where the frozen environment becomes very large.

The numerical integration used in ADF[36,37] is based on a partitioning of space into atomic polyhedra that are constructed as Voronoi cells around the atoms and the remaining "outer region". Inside the atomic polyhedra, a dense spherical grid

around the atom ensures an accurate integration of the Coulomb singularity of the nucleus, and in the outer region, few integration points are needed. Details of this grid generation are explained in ref 55.

In the new KSCED implementation, atomic polyhedra are only constructed for atoms that are within a certain distance from atoms in the nonfrozen system (4.0 Å in the present example). All other atoms in the frozen part are considered part of the outer region. This ensures a sufficient number of grid points for an accurate integration, where the integrand in eq 4 is nonnegligible; few integration points are created in those regions where the integrand vanishes because the basis functions, $\chi_{i,j}$, of the nonfrozen system are small. With the integration grid generated in this way, the number of grid points for larger environments no longer increases with the size of the frozen environment.

It is important to note that numerical integration over basis or fit functions of the frozen system is completely avoided. The (electronic) Coulomb part of the embedding potential

$$V_{\mathrm{emb}}^{\mathrm{Coulomb}}(\mathbf{r}) = \int \frac{\rho_{\mathrm{II}}(\mathbf{r}')}{|\mathbf{r}-\mathbf{r}'|}\,\mathrm{d}\mathbf{r}' \tag{5}$$

is calculated using density fitting, i.e., the electron density of the frozen environment $\rho_{\mathrm{II}}(\mathbf{r})$ is expressed as a linear combination of STO fit functions, χ^{fit}:

$$\rho_{\mathrm{II}}(\mathbf{r}) \approx \sum_i c_i \chi_i^{\mathrm{fit}}(\mathbf{r}) \tag{6}$$

These fit functions are centered on the atoms of the frozen environment. Integrals over these functions, as needed for $V_{\mathrm{emb}}^{\mathrm{Coulomb}}(\mathbf{r})$, can easily be calculated analytically.[37] The Coulomb potential has to be evaluated only on the integration grid in the nonfrozen system.

A further speedup of the calculations is achieved by the use of linear scaling techniques[56] to skip complete blocks of integration points for basis functions that are small on these parts of the grid.

With this improved implementation, for most parts of the calculation, the CPU time needed no longer depends on the size of the frozen environment. For large environments, the number of grid points is constant, even if the size of the frozen system is further increased. Therefore, the time needed for one SCF cycle and the time spent for the TDDFT calculation are also independent of the size of the frozen system.

There are two steps that still scale roughly linear with the size of the environment: the construction and fitting of the environment density and the calculation of the frozen density and its Coulomb potential in the grid points. Because the density of the environment is frozen during the SCF steps, these steps are only performed once at the beginning of the calculation. The frozen density and the corresponding Coulomb potential are then stored for further use.

Because of these changes, a large speedup of the embedding calculations could be achieved. Figure 3 shows the CPU times for calculations (on one processor of an SGI Altix 3700) of the five lowest excitations of aminocoumarin C151 solvated by 0−500 water molecules. The structure employed here is an arbitrary snapshot from a classical MD simulation. For the preparation of the frozen density, the innermost 50 water molecules were treated as flexible fragments with the geometries they have in the snapshot, and a uniform rigid structure (optimized in vacuo) was assumed for the outer water molecules (cf. ref 10).

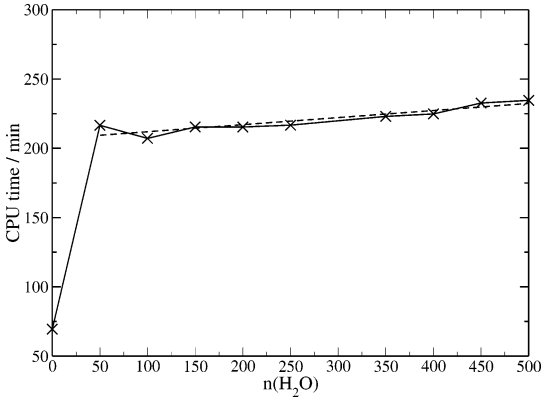

Figure 3. Total CPU times for calculations of the five lowest excitations of aminocoumarin C151 on one processor of an SGI Altix 3700 as a function of the number of frozen water molecules considered. The CPU times include the frozen-density preparation, embedded SCF, and embedded TDDFT steps. Additionally, a linear fit to the wall-clock times of the embedding calculations is shown.

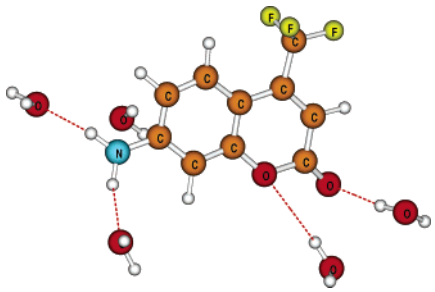

Figure 4. Cluster obtained as a substructure of an MD snapshot (see text), for which tests on specific interactions have been performed.

The frozen-density preparation step is reduced to a very small amount of the total CPU time and typically takes less than 10 min, even for the largest systems considered here. The calculation of the frozen density and its Coulomb potential in the grid points still shows an approximately linear increase in computer time with the size of the frozen system, whereas the time needed for one SCF cycle is constant (about 8 min in the present example). The effort for the TDDFT part is approximately 55 min for all embedded calculations for this snapshot, independent of the size of the solvent shell. The deviations between excitation energies calculated with the reduced grid and with a full integration grid are negligible (typically not larger than ≈0.0001 eV).

4. Specific Interactions with Frozen-Density Embedding

In ref 12, it was shown for DNA base pairs that shifts in excitation energies due to specific interactions, notably hydrogen bonding, can be reproduced with frozen-density embedding with an accuracy of 0.01−0.06 eV (in comparison to supermolecule calculations). To test effects of specific interactions in the present example, we took an arbitrary snapshot from the MD simulation in water, which will be described in more detail in section 7, and removed all but the five water molecules closest to the dye molecule from that structure. The resulting structure is shown in Figure 4. It can clearly be seen that at least four hydrogen bonds play a role for this structure.

We calculated the excitation energy for the $\pi \rightarrow \pi^*$ excitation of the C151 molecule plus the five water molecules both in a supermolecule calculation and by treating the five water molecules with frozen-density embedding. The results are presented in Table 1. The excitation energy for the isolated C151 molecule in the structure of this snapshot is 3.248 eV, which is

TABLE 1: Excitation Energies, E_{ex} (eV), of the Lowest ($\pi \rightarrow \pi^*$) Excitation of the Aminocoumarin C151·5H_2O Snapshot Depicted in Figure 4[a]

ρ_{II}	f & t[b]	exbas[c]	E_{ex} (eV)	ΔE_{ex} (eV)	f (au)
(isolated)		I	3.248		0.206
sum-of-fragments	0	I	3.036	−0.212	0.186
converged	0	I	3.046	−0.202	0.187
converged	1	I	3.007	−0.241	0.185
converged	2	I	2.997	−0.251	0.184
converged	0	I + II	3.046	−0.202	0.188
converged	1	I + II	3.007	−0.241	0.185
converged	2	I + II	2.994	−0.254	0.185
converged	3	I + II	2.993	−0.254	0.185
supermolecule		I + II	2.910	−0.338	0.196

[a] Supermolecule and frozen-density embedding with different ways to construct the frozen density have been used to calculate excitation energies. To see the effect of the water molecules, we also calculated the excitation energy for isolated aminocoumarin C151 in this particular structure (E_{ex}), the shifts with respect to this value (ΔE_{ex}), and the oscillator strengths (f). [b] The column "f & t" gives the number of freeze-and-thaw cycles used in the construction of the frozen density. [c] In column "exbas", it is shown whether the basis functions of system I (C151) only or those of both systems (I and II; II = 5H_2O) have been used to calculate the excitation energies.

shifted to 3.036 eV if the effect of the water molecules is included by a sum-of-fragment density. This sum-of-fragment approach does not introduce a considerable error in the preparation of the frozen density, as can be seen from the excitation energy of 3.046 eV for a water density from a converged SCF. This is in line with the observations in ref 10 but is also not very surprising in the present example of five weakly interacting water molecules.

A significant change arises from the first freeze-and-thaw cycle,[28] where the density of the five H_2O molecules is obtained from a calculation in which the density of the aminocoumarin molecule is kept frozen. Freezing this "polarized" density causes the excitation energy to go down to 3.007 eV. A second freeze-and-thaw cycle has only a minor effect and yields an excitation energy of 2.997 eV.

We repeated these freeze-and-thaw cycles using the combined basis sets of the systems I (C151) and II (the five water molecules), i.e., the basis set of the supermolecule. The differences in the excitation calculations with the basis set of system I only are negligible. In this case, we also performed a third freeze-and-thaw iteration, which led to a change of 0.001 eV with respect to the previous cycle, thus proving that no additional changes arise from further relaxation cycles.

Finally, we carried out a supermolecule calculation, which resulted in an excitation energy of 2.910 eV. This is 0.083 eV lower than the most sophisticated embedding calculation. It has been mentioned in ref 10 that, in general, the supermolecule calculations cannot be considered a strict benchmark for the frozen-density calculations, which was mainly due to the fact that those particular supermolecule calculations were plagued by artificial mixings with charge-transfer excitations. These mixings seem to be less important in this study because of the low excitation energy of the $\pi \rightarrow \pi^*$ excitation in aminocoumarin C151 (see, however, the comments at the end of section 6).

The frozen-density embedding in its most elaborate form is able to recover ca. 75% of the effect of the five water molecules on the excitation energies, which is a significant amount. The remaining discrepancy in comparison to the supermolecule calculation in this case is most likely due to the fact that the hydrogen-bonded water molecules directly contribute to the excitation; i.e., the assumption that the excitation is strictly localized to the aminocoumarin may not be completely valid. To also model the participation of orbitals of the hydrogen-bonded water molecules in the linear response, they have to be explicitly included into the embedded system.

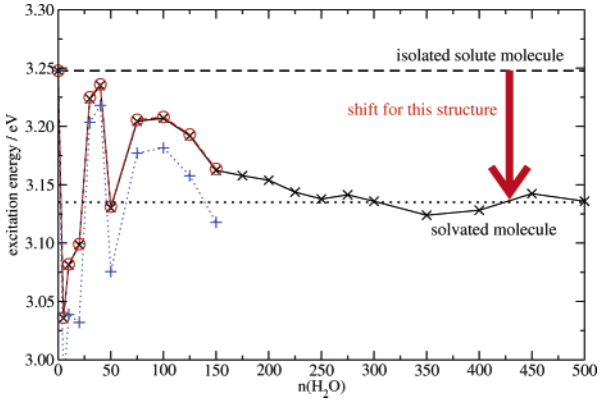

Figure 5. Excitation energy of aminocoumarin C151 as a function of the size of the (water) solvent shell considered in the frozen-density calculation for an arbitrary snapshot from an MD simulation. Three different basis sets have been used for the frozen density: (i) DZ (dotted line/+ symbol), (ii) DZP (solid line/× symbol), (iii) TZP (dashed line/○ symbol).

Table 1 also shows the oscillator strengths for the different types of calculations. It can be seen that both frozen-density and supermolecule calculations predict lower oscillator strengths for the solvated molecule than for the isolated one. The embedding calculations yield a larger change than the supermolecule calculations, and relaxation does not improve this situation. A reason may be that the intensities are more affected by the confinement of the response than the excitation energies are.

5. Appropriate Size of the Solvation Shell

To check the convergence of the excitation energy for the $\pi \rightarrow \pi^*$ excitation of aminocoumarin C151 with the size of the solvation shell, an example snapshot from the (periodic structure) MD simulation was taken, from which substructures were constructed and in which the n water molecules closest to the solute molecule were included in the frozen density. The criterion to determine the nearest neighbor molecules in this case was the minimum distance between a pair of atoms of the solute and the solvent molecule under consideration. The same snapshot was taken in section 4 to extract the structure of the C151·5H_2O cluster.

Substructures with up to 500 water molecules, i.e., up to 1500 atoms, in the frozen density were used. Excitation energies are given in Figure 5. As has been shown in section 4, the specific interactions due to the nearest five water molecules, even if treated as frozen electron density in KSCED, lead to a strong decrease of the excitation energy from 3.25 eV for the isolated dye molecule to 3.04 eV. For structures with 10−20 water molecules, the excitation energy increases a bit to 3.08 and 3.10 eV before a rather large step to 3.22 eV when 30 water molecules are included. From the irregular behavior for up to 50 water molecules, it can be seen that quite a large first solvation shell has to be considered in this case. From 75 water molecules on, a more regular behavior can be observed, in which the excitation energy goes down from ca. 3.20 to 3.16 eV for 150 water molecules. The influence of more water molecules is small but not completely negligible. The excitation energy goes down to 3.14 eV for a solvent shell of 225 solvent molecules, and from there on, it remains at 3.13 ± 0.01 eV for all structures studied. Using 300 solvent molecules, i.e., 900

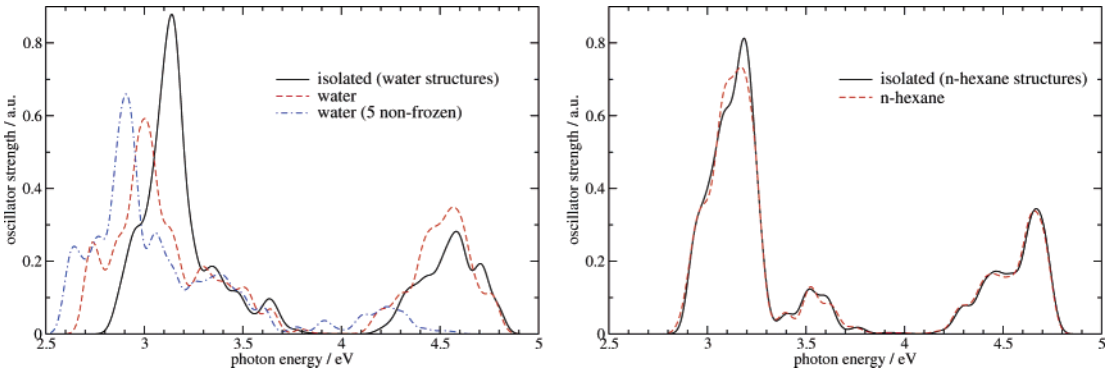

Figure 6. Simulated spectra for aminocoumarin C151 in solution based on reduced sets of 50 snapshots. Water (left) and *n*-hexane (right) have been considered as solvents. Each individual transition is represented by a Gaussian curve of half-width 0.08 eV. Spectra in which the solvent is either included in a frozen-density calculation or completely omitted are shown. In the latter case, only the structural effects of the dynamics in solution affect the spectrum. For water, we also show a simulation in which the five nearest water molecules are included in the embedded (nonfrozen) system. In this simulation, the band at the high-frequency end of the spectrum is not obtained because the number of excited states in the calculation was restricted to five and additional excitations arise because of the water molecules.

atoms, in the frozen part should therefore be enough to converge the excitation energies. The radius of the solvent shell is approximately 4.5 Å for 50 water molecules, 10 Å for 300 water molecules, and 12 Å for 500 water molecules.

For structures with up to 150 water molecules, we also used the TZP and DZ basis sets from the ADF basis set library for the frozen water molecules to check their effect on the excitation energies. As can be seen, the DZ basis set leads to an underestimation of the excitation energies for each structure of about 0.04 ± 0.02 eV. The difference between the DZP and TZP basis sets, however, is hardly visible. Therefore, we conclude that the DZP basis set for the frozen-density system is large enough to converge the excitation energies.

Also, for *n*-hexane as a solvent, we tested the influence of the size of the solvent shell on the excitation energy. In this case, the variation is very small. The first five solvent molecules (100 atoms in total) cause a shift in the excitation energy of −0.005 eV, and adding further solvent molecules leads to variations in the shift from −0.006 to −0.002 eV. When the number of solvent molecules is increased from 40 (800 atoms) to 45 (900 atoms), the excitation energy changes only from 3.1295 to 3.1299 eV.

6. Validation of the Solvent Model

The calculation of solvatochromic shifts requires sampling over the different possible structures of the solute and the surrounding solvent. In this section, we want to validate our solvent model using a small set of 50 snapshots of C151 in solution for each solvent by comparing different types of embedding calculations. An extended statistical sampling with 400 snapshots from eight independent trajectories follows in the next section, which shows that the results obtained in this section are accidentally closer to experiment. Additionally, we try to separate the structural and electronic contributions to changes in the excitation energies.

To this end, canonical ensemble (NVT) classical dynamics simulations, as explained in section 2, were performed. The MD simulations for aqueous solution were carried out at a temperature of 300 K, with a cubic box of length 25 Å, containing one aminocoumarin dye molecule and 513 water molecules, leading to a density of 1.0066 kg/L. Starting from a random water structure around the aminocoumarin dye, we first optimized the structure and then equilibrated for 50 ps, heated the system to 500 K, cooled it to 300 K, and equilibrated again for 50 ps. After this preparation, a trajectory of 50 ps was generated with a time step of 2 fs. Every picosecond a snapshot of the system was taken for the statistical analysis. No rigid bond constraints were used in the simulations presented here. However, an additional trajectory, in which we used a Shake-like algorithm[57] to constrain bonds involving hydrogen atoms, resulted in only slight changes compared to those of the trajectory discussed here (the average excitation energy for a set of 50 structures changed by less than 0.03 eV). The MD simulations with *n*-hexane as a solvent were carried out in the same manner. We also used a cubic box of length 25 Å with a density of the solution of 0.6745 kg/L (71 *n*-hexane molecules). Because this is a bit higher than the density of pure *n*-hexane at the simulation temperature and because no accurate information about the density of the solution studied here is available, we performed an additional test with the slightly lower density of 0.6596 kg/L (cubic box of length 25.1881 Å). No significant changes could be observed in the resulting spectra.

For the snapshots from these simulations, a substructure from the periodic-boundary simulation was created, in which the nearest 300 solvent molecules were taken into account in the case of water as a solvent and the nearest 45 solvent molecules were taken into account in the case of *n*-hexane. This amounts to 900 atoms in the frozen-density system in both cases. For the preparation of the frozen-density system in the former case, the innermost 50 water molecules were treated as flexible fragments (geometries taken from the snapshots) and a uniform rigid structure (optimized in vacuo) was used for the outer water molecules (cf. section 3). No rigid structures were assumed for the *n*-hexane molecules.

First, we computed the shift in excitation energies for C151 in *n*-hexane compared to the vertical $\pi \rightarrow \pi^*$ excitation energy of the optimized, isolated molecule (3.238 eV). To separate the structural effect due to the dynamics in solution and the electronic effect due to the frozen density, we performed two series of excitation calculations: in the first, we removed all solvent molecules from the snapshots, whereas we kept them in the second. The first series, which includes only the structural effect, resulted in an average excitation energy of 3.096 eV, which is 0.142 eV lower than the vertical excitation energy for the isolated molecule. In contrast to this, the electronic effect in *n*-hexane is negligible. If the *n*-hexane molecules are included by frozen-density embedding, the average excitation energy changes by only 0.004 eV to reach a value of 3.092 eV. The spectra simulated in this way are shown in Figure 6.

TABLE 2: Average Excitation Energies and Solvent Shifts (eV) for the $\pi \rightarrow \pi^*$ Excitation of Aminocoumarin C151[a]

structure C151	solvent model	E_{ex} (eV)
isolated, opt.		3.238
simulation *n*-hexane		3.096
simulation *n*-hexane	45 *n*-hexane (fr, nonrel)	3.092
simulation H_2O		3.085
simulation H_2O	300 H_2O (fr, nonrel)	2.955
simulation H_2O	5 H_2O (fr, rel), 295 H_2O (fr, nonrel)	2.930
simulation H_2O	10 H_2O (fr, rel), 290 H_2O (fr, nonrel)	2.923
simulation H_2O	10 H_2O (fr, fully rel), 290 H_2O (fr, nonrel)	2.916
simulation H_2O	5 H_2O (nonfr), 295 H_2O (fr, nonrel)	2.862

[a] They are obtained from an analysis of a reduced set of 50 snapshots of MD simulations for this molecule in water and *n*-hexane, respectively. For comparison, we also present calculations in which the solvent molecules have been removed in the excitation calculation so that only the structural effect of the dynamics in solution is monitored. The acronym "fr" stands for frozen and nonrelaxed solvent molecules; "rel" means frozen and relaxed (polarized by the C151 density) solvent molecules; "fully rel" means frozen and fully relaxed solvent molecules (polarized by C151 and the outer water molecules); and "nonfr" denotes nonfrozen solvent molecules (included in the embedded system).

In ref 8, the vertical excitation energy of the isolated molecule was taken as a reference value to compute the "solvent shift" for solvation in water, which was then compared to the experimental shift between water and *n*-hexane (the latter being a solvent where both specific and nonspecific solvent effects are expected to be small). In view of the difference of 0.146 eV in our calculation between the isolated molecule and the average excitation energy in *n*-hexane, we think that this is an oversimplification. This is mainly due to the fact that the (dynamic) structural effect is neglected in a (static) vertical excitation calculation. This also holds true when comparing the solvent shift to a shift between experimental gas-phase and solution spectra because gas-phase dynamics may also change the average excitation energy by 0.1−0.2 eV compared to vertical excitation energies, as is known from other CPMD[10] or vibronic coupling simulations.[27]

We performed similar calculations for the snapshots obtained with water as a solvent. Considering the pure structural effect, we obtained an average excitation energy of 3.085 eV, which is comparable to *n*-hexane. This suggests that, within our model for the dynamics, there are no significant structural differences in the solute molecule itself for the different solvents. In contrast to *n*-hexane, however, the electronic effect is more important for the aqueous solution. Modeling this electronic effect by the frozen-density embedding including 300 frozen water molecules yields an average excitation energy of 2.955 eV, such that structural (−0.153 eV) and electronic effects (−0.130 eV) are of similar magnitude.

The solvent shift of −0.137 eV between *n*-hexane and water calculated from these limited statistics, though qualitatively correct, considerably underestimates the experimental shift of −0.22 eV. The tests in section 4 showed that the frozen-density embedding, especially in its simplest form (i.e., without relaxation), may have some problems in accurately modeling the effect of hydrogen-bonded water molecules. This could be improved, but in the present case not completely cured, by using at least one freeze-and-thaw cycle to polarize the frozen density. There is, however, a fundamental problem when the sum-of-fragment approach, introduced in ref 10, is used to generate the frozen-solvent density: we can only polarize the frozen density during an SCF for the solvent system. The results in ref 12 suggest that polarization is most important in those cases, where direct hydrogen bonding between the frozen and the embedded system becomes important. We therefore tested the following hybrid approach: We chose a set of solvent molecules which are close to the solute, typically only five to ten molecules in the case of water, and calculated their density in a KSCED calculation, in which the density of the isolated aminocoumarin C151 is kept frozen. Then, we combined the density of this polarized fragment with the density of all remaining solvent molecules using the simple sum-of-fragment approach. The resulting density was frozen and used in a KSCED calculation on aminocoumarin C151. This partial relaxation leads to an average excitation energy of 2.930 eV when the nearest five water molecules are polarized and of 2.923 eV when the nearest ten water molecules are relaxed, thus improving the shift between *n*-hexane and the water solution from −0.137 to −0.162 or −0.169 eV, respectively. The small change from five to ten polarized water molecules confirms that polarization is only needed for the closest solvent molecules that show the strongest interactions with the solute. We also tested the effect of relaxing the ten nearest water molecules, with respect not only to the frozen C151 density but also to the frozen density of the remaining water molecules, before this relaxed density was combined with the other water molecules and again used in a KSCED calculation on aminocoumarin C151. This yielded an average excitation energy of 2.916 eV, corresponding to a solvent shift of −0.176 eV.

According to the analyses in section 4, the restriction of the response to the embedded system can be another significant source of error in the present case. Because of this restriction, changes in the solvent electron density upon excitation cannot be described. A big advantage of the embedding scheme is that the embedded system can always be extended to include the nearest solvent molecules if we have an indication that they might take part in the excitation process. This leads to a shell-like approach, which is shown in Figure 7: There are three layers of water molecules in the system, of which the innermost is treated explicitly (or by relaxation, if sufficient). The next layer consists of normal frozen solvent molecules, which complete (at least) the first solvation shell. The third layer is formed by rigid water molecules modeling outer solvation shells.

We tested this for the simulation in water and included the five water molecules closest to the dye molecule in the nonfrozen system, whereas the remaining 295 water molecules for each snapshot were described by the frozen-density embedding scheme. The effect is similar to the results in section 4: The average excitation energy for the $\pi \rightarrow \pi^*$ excitation drops to 2.862 eV, which is 0.093 eV lower than that of the sum-of-fragment calculation. This corresponds to a solvent shift between *n*-hexane and water of 0.230 eV for this limited set of snapshots, which agrees within 0.01 eV with the experimental shift. The standard error in the average excitation energies is still larger than 0.02 eV in this case. The combination of five explicit water molecules in the embedded system with 295 frozen water molecules thus appears appropriate to be used in a more extensive statistical sampling (see below). Including more water molecules in the nonfrozen region appears neither necessary nor adequate. Such water molecules, which are not hydrogen-bonded to the dye molecule, will not directly contribute to the $\pi \rightarrow \pi^*$ excitation. The calculations with partially polarized water densities already demonstrate that the influence of the nearest five water molecules on the average excitation energy is much larger than that of the next five water molecules.

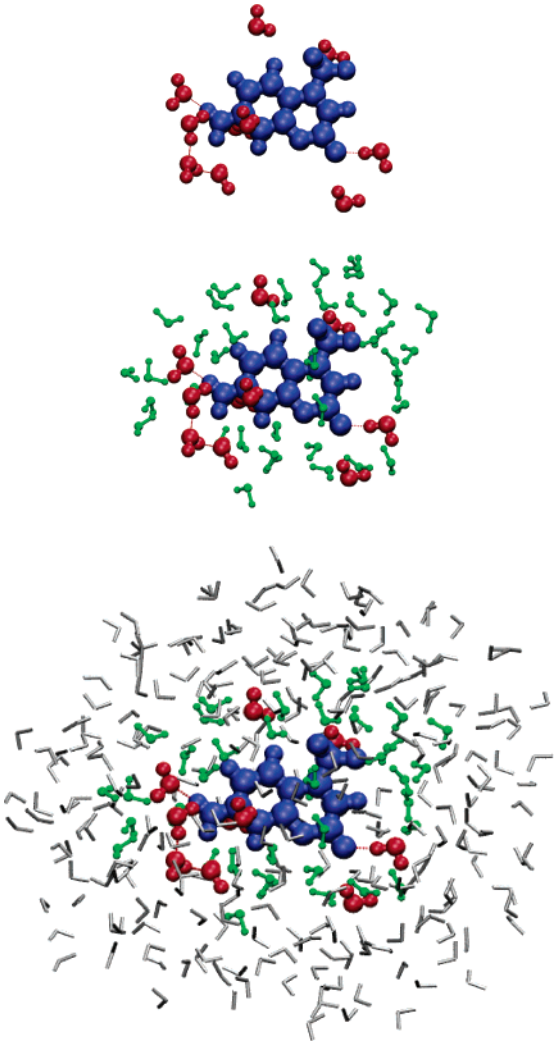

Figure 7. Shell structure in frozen-density embedding calculations. Top: The innermost solvent molecules (red), for which hydrogen bonding to the solute (blue) is expected, can be included in the embedded system, or partial relaxation can be used for them. Middle: To complete the first solvation shell, flexible, solvent molecules (green) are added with structures according to the snapshot of the dynamics and with frozen density. Bottom: Outer solvation shells are modeled by rigid water molecules (grey). Graphics: VMD.[58]

Additionally, the calculations with more nonfrozen water molecules would suffer from two problems: First, the computer time still shows the scaling behavior of conventional DFT/TDDFT calculations with respect to the number of atoms in the nonfrozen region, so the calculations get considerably more expensive if many water molecules are included in the embedded part. Secondly, and even more severe, explicit water molecules increase the risk of artificially low-lying charge-transfer excitations from water−oxygen lone pairs to the π^* orbital of the aminocoumarin. Even with only five explicit water molecules, such excitations occur in rare cases. They can also affect the desired excitations by spurious mixings[10] and make the identification of these excitations cumbersome.

7. Spectra Simulations

To improve our statistical analysis, we use 8 trajectories as explained in section 6 for every solvent, leading to 400 snapshots in each case. Between the individual trajectories, we heat the system to 500 K, cool it to 300 K, and reequilibrate for 50 ps. In the last section, it was shown that it is necessary to include water molecules which interact via hydrogen bonds with the aminocoumarin explicitly into the embedded system. Therefore, we use five explicitly nonfrozen and 295 unpolarized frozen water molecules for water as a solvent. For comparison, we also perform a calculation in which all water molecules are frozen and unpolarized. For *n*-hexane, we only use this simple scheme because electronic effects are very small in that case anyway.

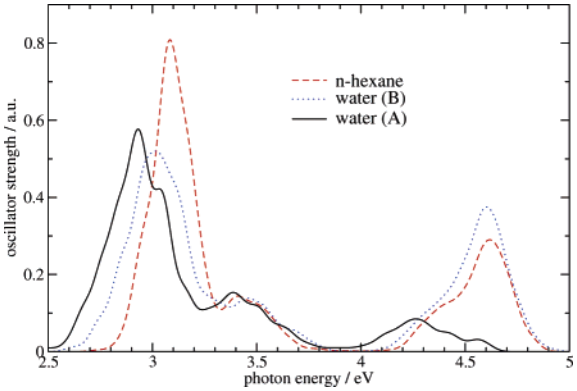

Figure 8. Simulated spectra for aminocoumarin C151 in solution. Water and *n*-hexane have been considered as solvents. Each individual transition is represented by a Gaussian curve of half-width 0.08 eV. For water, two simulations have been carried out: (A) 5 nonfrozen and 295 frozen water molecules and (B) all 300 water molecules frozen. In the former simulation, the band at the high-frequency end of the spectrum is not obtained because the number of excited states in the calculation is restricted to 5 and additional excitations arise because of the water molecules.

TABLE 3: Average Excitation Energies and Solvent Shifts (eV) for the $\pi \rightarrow \pi^*$ Excitation of Aminocoumarin C151[a]

	embedding (SAOP/TZP/DZP)	QM/MM-CPMD[b] (BLYP)	exptl[c]
isolated, opt.	3.24	3.32	
n-hexane	3.07		3.70
water (A)	2.90	2.99	3.48
water (B)	2.99		
shift *n*-hexane−water (A)	−0.17		−0.22
shift *n*-hexane−water (B)	−0.08		
shift isolated−water (A)	−0.33	−0.33	
shift isolated−water (A)	−0.25		

[a] They are obtained from an analysis of 400 snapshots of MD simulations for this molecule in water and *n*-hexane, respectively. Two simulations have been carried out for water: (A) with five water molecules included in the embedded system and 295 frozen H_2O molecules and (B) with all 300 water molecules frozen. For comparison, we give the shift with respect to the vertical excitation energy of the optimized isolated structure. We also include the results from a QM/MM-CPMD study (all water molecules are treated in MM fashion there).[8] [b] See ref 8. [c] See ref 18.

In Figure 8, we present the spectra resulting from 400 snapshots of the simulation in water and in *n*-hexane. Average excitation energies and solvent shifts calculated from these data are presented in Table 3. All solvent shifts here are extracted from average excitation energies, but using other methods to extract the mean values (cf. ref 10) changes this shift only on the order of 0.01−0.02 eV.

The simulation for *n*-hexane yields an average excitation energy of 3.07 eV, which is ca. 0.02 eV lower than for the smaller test set studied in section 6 and 0.17 eV lower than the vertical excitation energy for the optimized, isolated structure. The average excitation energy in water is 2.90 eV for the recommended solvent model including five nonfrozen water molecules, which is ca. 0.04 eV higher than that for the limited

statistics in the last section. Also, for the simpler model with 300 frozen water molecules, the larger statistics increases the average excitation energy by about 0.03−0.04 (compared to the single trajectory) to 2.99 eV.

The calculated solvent shift from *n*-hexane to water is −0.17 eV when including five nonfrozen water molecules, which is in satisfactory agreement with the experimental shift of −0.22 eV. The simple embedding technique with all 300 water molecules frozen also shows a clear shift in the negative direction, but its magnitude is somewhat underestimated with only −0.08 eV. Because of the standard errors in the average excitation energies (0.005−0.008 eV), the statistical error estimated for the solvent shifts is ca. ±0.01 eV.

In Table 3, we also calculate the shifts between the isolated molecule and the molecule solvated in water. Although this shift lacks a direct physical meaning, it allows a comparison to the QM/MM-CPMD study in ref 8. With five nonfrozen water molecules, the shift between isolated structures and aqueous solution in our calculation is identical to that in ref 8, where all water molecules were treated with a classical model (−0.33 eV). The simple embedding technique (300 frozen water molecules) instead yields a value of −0.25 eV for this shift. If we would use the vertical excitation energy of the optimized, isolated molecule as a first approximation to the average excitation energy in a nonpolar solvent such as *n*-hexane, we would have to conclude that the simpler embedding model with 300 frozen water molecules yields the better results. The direct comparison of the average excitation energies in the different solvents reveals, however, that this is not the case.

8. Conclusions

In this study, we could show that frozen-density embedding is a very efficient method for modeling solvent effects. Because of an optimized grid generation scheme and the combination of linear-scaling techniques with the frozen-density embedding as well as the efficient generation of solvent densities by a sum-of-fragments approach, the size of the explicitly modeled environment could be extended to solvent shells including more than 1000 atoms. Because such calculations are easily possible, even on single CPUs of a modern PC, modeling general solvent effects by an evaluation of several hundreds of snapshots including large solvation shells (900 atoms in the present example) becomes feasible. Explicit solvent models for systems of this size were, up to now, restricted to (semi) empirical models, whereas frozen-density embedding does not require any empirical information, apart from the usual parametrization in the density functionals.

A full simulation of spectra including the influence of the solvent requires us to take the dynamical effects into account by sampling over a statistical set of snapshots in solution. In the present example, this was accomplished by a combination of classical molecular dynamics simulations and subsequent frozen-density calculations. Hence, the structures used in our study still rely on empirical information whereas the excitation energies do not. A more consistent treatement would require *first-principles* CPMD to generate the snapshots.[10] However, such entirely quantum chemical simulations appear to be too costly for molecules which require rather large solvation shells. In particular, if the solvent molecules are also of appreciable size (like *n*-hexane in this study), the required box size would become too large for CPMD simulations. A compromise might be found by using QM/MM-CPMD simulations to generate the snapshots, followed by frozen-density embedding calculations of the excitation energies.

We could show that the vertical excitation energy of the isolated molecule is not a well-defined reference for the computation of solvatochromic shifts in a polar medium with respect to a nonpolar one. For a direct comparison to experimental shifts in different media, the absorption spectra should be modeled in both solvents and then be compared. For aminocoumarin C151, the structural effects due to the dynamics in solution lead to similar spectra for both water and *n*-hexane as solvents.

Although almost no electronic effect on the excitation energies arises in the *n*-hexane solution for aminocoumarin C151, such an effect is clearly visible for an aqueous solution. A considerable change in the excitation energies is induced by water molecules which are hydrogen-bonded to aminocoumarin C151. This is reproduced to a large extent by an all-frozen environment, although supermolecule calculations predict a somewhat larger effect. The spectral simulations show that the calculated solvent shift between the two different solvents is too small if all water molecules are kept frozen, but it is still qualitatively correct. Our tests on a limited set of 50 snapshots clearly demonstrate that the results can be improved by a relaxation of the frozen density. Although this relaxation usually requires a full SCF for the frozen system, we devised a method to combine a partial relaxation of the innermost solvent shell with the sum-of-fragment approach for the construction of the frozen density.

An inclusion of a few solvent molecules in the embedded region remains important in those cases where the first solvation shell takes part in the response of the system because the frozen-density embedding TDDFT approach in the current form ignores such contributions of the frozen part. In the present case, the magnitude of the experimental shift of −0.22 eV is reproduced within 0.05 eV when the closest water molecules are included in the embedded system. A quantitative prediction of solvent shifts is thus efficiently possible by this QM/QM embedding, even if the response is not strictly localized on the solute molecule.

Acknowledgment. The authors would like to thank Dr. Lucas Visscher for helpful discussions. J.N. gratefully acknowledges funding by a Forschungsstipendium of the Deutsche Forschungsgemeinschaft (DFG). C.R.J. and E.J.B. thank The Netherlands Organization for Scientific Research (NWO) for financial support via the TOP program. T.A.W. was supported by the Swiss National Scientific Foundation (SNSF) and OFES acting as the Swiss COST office.

References and Notes

(1) Han, W.-G.; Liu, T.; Himo, F.; Toutchkine, A.; Bashford, D.; Hahn, K. M.; Noodleman, L. *ChemPhysChem* **2003**, *4*, 1084−1094.

(2) Liu, T.; Han, W.-G.; Himo, F.; Ullmann, G. M.; Bashford, D.; Toutchkine, A.; Hahn, K. M.; Noodleman, L. *J. Phys. Chem. A* **2004**, *108*, 3545−3555.

(3) Car, R.; Parrinello, M. *Phys. Rev. Lett.* **1985**, *55*, 2471−2474.

(4) Odelius, M.; Kirchner, B.; Hutter, J. *J. Phys. Chem. A* **2004**, *108*, 2044−2052.

(5) Bernasconi, L.; Sprik, M.; Hutter, J. *J. Chem. Phys.* **2003**, *119*, 12417−12431.

(6) Bernasconi, L.; Sprik, M.; Hutter, J. *Chem. Phys. Lett.* **2004**, *394*, 141−146.

(7) Röhrig, U. F.; Frank, I.; Hutter, J.; Laio, A.; VandeVondele, J.; Rothlisberger, U. *ChemPhysChem* **2003**, *4*, 1177−1182.

(8) Sulpizi, M.; Carloni, P.; Hutter, J.; Rothlisberger, U. *Phys. Chem. Chem. Phys.* **2003**, *5*, 4798−4805.

(9) Wesolowski, T. A.; Warshel, A. *J. Phys. Chem.* **1993**, *97*, 8050−8053.

(10) Neugebauer, J.; Louwerse, M. J.; Baerends, E. J.; Wesolowski, T. A. *J. Chem. Phys.* **2005**, *122*, 094115.

(11) Casida, M. E.; Wesolowski, T. A. *Int. J. Quantum Chem.* **2004**, *96*, 577−588.

(12) Wesolowski, T. A. *J. Am. Chem. Soc.* **2004**, *126*, 11444−11445.
(13) Osted, A.; Kongsted, J.; Mikkelsen, K. V.; Christiansen, O. *J. Phys. Chem. A* **2004**, *108*, 8646−8658.
(14) Besley, N. A.; Oakley, M. T.; Cowan, A. J.; Hirst, J. D. *J. Am. Chem. Soc.* **2004**, *126*, 13502−13511.
(15) Besley, N. A. *Chem. Phys. Lett.* **2004**, *390*, 124−129.
(16) *Dye Lasers*, 3rd ed.; Schäfer, F. P., Ed.; Springer: Berlin, 1990.
(17) *New Trends in Fluorescence Spectroscopy: Applications to Chemical and Life Sciences*; Valeur, B., Brochon, J.-C., Eds.; Springer: Berlin, 2001.
(18) Gustavsson, T.; Cassara, L.; Gulbinas, V.; Gurzadyan, G.; Mialocq, J.-C.; Pommeret, S.; Sorgius, M.; van der Meulen, P. *J. Phys. Chem. A* **1998**, *102*, 4229−4245.
(19) Jones, G., II; Jackson, W. R.; yoo Choi, C.; Bergmark, W. R. *J. Phys. Chem.* **1985**, *89*, 294−300.
(20) Moylan, C. R. *J. Phys. Chem.* **1994**, *98*, 13513−13516.
(21) Cave, R. J.; Burke, K.; Castner, E. W., Jr. *J. Phys. Chem. A* **2002**, *106*, 9294−9305.
(22) Cave, R. J.; Castner, E. W., Jr. *J. Phys. Chem. A* **2002**, *106*, 12117−12123.
(23) Ando, K. *J. Chem. Phys.* **1997**, *107*, 4585−4596.
(24) Horn, M. L.; Gardecki, J. A.; Papazyan, A.; Maroncelli, M. *J. Phys. Chem.* **1995**, *99*, 17311−17337.
(25) Dierksen, M.; Grimme, S. *J. Chem. Phys.* **2004**, *120*, 3544−3554.
(26) Dierksen, M.; Grimme, S. *J. Phys. Chem. A* **2004**, *108*, 10225−10237.
(27) Neugebauer, J.; Baerends, E. J.; Nooijen, M. *J. Phys. Chem. A* **2005**, *109*, 1168−1179.
(28) Wesolowski, T. A.; Weber, J. *Int. J. Quantum Chem.* **1997**, *61*, 303.
(29) Parr, R. G.; Yang, W. *Density-Functional Theory of Atoms and Molecules;* Oxford University Press: Oxford, 1989.
(30) Cortona, P. *Phys. Rev. B* **1991**, *44*, 8454−8458.
(31) Wesolowski, T. A.; Chermette, H.; Weber, J. *J. Chem. Phys.* **1996**, *105*, 9182−9190.
(32) Wesolowski, T. A. *J. Chem. Phys.* **1997**, *106*, 8516−8526.
(33) Perdew, J. P. In *Electronic Structure of Solids*; Ziesche, P., Eschrig, H., Eds.; Akademie Verlag: Berlin, 1991.
(34) Lembarki, A.; Chermette, H. *Phys. Rev. A* **1994**, *50*, 5328−5331.
(35) Becke, A. D. *Phys. Rev. A* **1988**, *38*, 3098−3100.
(36) *Amsterdam Density Functional Program*; Theoretical Chemistry, Vrije Universiteit: Amsterdam. http://www.scm.com.
(37) te Velde, G.; Bickelhaupt, F. M.; Baerends, E. J.; Fonseca Guerra, C.; van Gisbergen, S. J. A.; Snijders, J. G.; Ziegler, T. *J. Comput. Chem.* **2001**, *22*, 931−967.
(38) Wang, J.; Wolf, R. M.; Caldwell, J. W.; Kollman, P. A.; Case, D. A. *J. Comput. Chem.* **2004**, *25*, 1157−1174.
(39) Jorgensen, W. L.; Chandrasekhar, J.; Madura, J. D. *J. Chem. Phys.* **1983,** *79*, 926−935.
(40) Ponder, J. W. TINKER − Software Tools for Molecular Design, Version 4.2, 2004. http://dasher.wustl.edu/tinker.
(41) Ponder, J. W.; Richards, F. M. *J. Comput. Chem.* **1987**, *8*, 1016−1024.
(42) Swart, M.; van Duijnen, P.; Snijders, J. *J. Comput. Chem.* **2001**, *22*, 79−88.
(43) Perdew, J. P. *Phys. Rev. B* **1986**, *33*, 8822−8824.
(44) Schipper, P. R. T.; Gritsenko, O. V.; van Gisbergen, S. J. A.; Baerends, E. J. *J. Chem. Phys.* **2000**, *112*, 1344−1352.
(45) Gritsenko, O. V.; Schipper, P. R. T.; Baerends, E. J. *Chem. Phys. Lett.* **1999**, *302*, 199−207.
(46) Gritsenko, O. V.; Schipper, P. R. T.; Baerends, E. J. *Int. J. Quantum Chem.* **2000**, *76*, 407−419.
(47) Grüning, M.; Gritsenko, O. V.; van Gisbergen, S. J. A.; Baerends, E. J. *J. Chem. Phys.* **2002**, *116*, 9591−9601.
(48) Casida, M. E. Time-Dependent Density Functional Response Theory for Molecules. In *Recent Advances in Density Functional Methods Part I*; Chong, D. P., Ed.; World Scientific: Singapore, 1995.
(49) van Gisbergen, S. J. A.; Snijders, J. G.; Baerends, E. J. *Comput. Phys. Commun.* **1999**, *118*, 119−138.
(50) Autschbach, J.; Ziegler, T. *Coord. Chem. Rev.* **2003**, *238/239*, 83−126.
(51) Wesolowski, T.; Warshel, A. *J. Phys. Chem.* **1994**, *98*, 5183−5187.
(52) Wesolowski, T.; Muller, R. P.; Warshel, A. *J. Phys. Chem.* **1996**, *100*, 15444−15449.
(53) Hong, G.; Strajbl, M.; Wesolowski, T.; Warshel, A. *J. Comput. Chem.* **2000**, *21*, 1554−1561.
(54) Choly, N.; Lu, G. *Phys. Rev. B* **2005**, *71*, 094101.
(55) te Velde, G.; Baerends, E. J. *J. Comput. Phys.* **1992**, *99*, 84−98.
(56) Fonseca Guerra, C.; Snijders, J. G.; te Velde, G.; Baerends, E. J. *Theor. Chem. Acc.* **1998**, *99*, 391−403.
(57) van Gunsteren, W.; Berendsen, H. *Mol. Phys.* **1977**, *34*, 1311−1327.
(58) Humphrey, W.; Dalke, A.; Schulten, K. *J. Mol. Graphics* **1996**, *14.1*, 33−38.